$A_2Bi_8Se_{13}$ (A = Rb, Cs), $CsBi_{3.67}Se_6$, and $BaBi_2Se_4$: New Ternary Semiconducting Bismuth Selenides

Lykourgos Iordanidis,[†] Paul W. Brazis,[‡] Theodora Kyratsi,[†] John Ireland,[‡] Melissa Lane,[‡] Carl R. Kannewurf,[‡] Wei Chen,[§] Jeffrey S. Dyck,[§] Ctirad Uher,[§] Nishant A. Ghelani,[||] Tim Hogan,[||] and Mercouri G. Kanatzidis*[,†]

Department of Chemistry and Center for Fundamental Materials Research, Michigan State University, East Lansing, Michigan 48824, Department of Electrical and Computer Engineering, Northwestern University, Evanston, Illinois 60208, Department of Physics, University of Michigan, Ann Arbor, Michigan 48109, and Department of Electrical and Computer Engineering, Michigan State University, East Lansing, Michigan 48824

Received September 12, 2000. Revised Manuscript Received October 25, 2000

$Rb_2Bi_8Se_{13}$ (**I**), $Cs_2Bi_8Se_{13}$ **(II)**, $CsBi_{3.67}Se_6$ **(III),** and $BaBi_2Se_4$ (**IV**) were synthesized by direct combination reactions of the A/Se (A = Rb, Cs, Ba) and Bi_2Se_3 at ≥650 °C. Their structures were determined by single-crystal X-ray diffraction. $Rb_2Bi_8Se_{13}$ and $Cs_2Bi_8Se_{13}$ are isostructural and crystallize in the monoclinic space group $P2_1/m$ (No. 11) with a = 13.4931(4) Å, b = 4.1558(3) Å, c = 24.876(2) Å, β = 96.571(4)°, R1 = 0.0577, and wR2 = 0.1159 [$I > 2\sigma(I)$] for **I** and a = 13.704(1) Å, b = 4.1532(4) Å, c = 25.008(2) Å, β = 96.848(2)°, R1 = 0.0497, and wR2 = 0.1123 [$I > 2\sigma(I)$] for **II**. $CsBi_{3.67}Se_6$ crystallizes in the orthorhombic space group *Pnma* (No. 62) with a = 23.421(4) Å, b = 4.1877(8) Å, c = 13.710(3) Å, R1 = 0.0611, and wR2 = 0.1384 [$I > 2\sigma(I)$]. $BaBi_2Se_4$ crystallizes in the hexagonal space group $P6_3/m$ (No. 176) with a = 26.157(1) Å, c = 4.3245(3) Å, R1 = 0.0371, and wR2 = 0.0817 [$I > 2\sigma(I)$]. The structure of $A_2Bi_8Se_{13}$ features a three-dimensional framework consisting of wide rectangular NaCl-type infinite rods, running parallel to the b-axis, which are stitched together by CdI_2- and Sb_2Se_3-type fragments. The NaCl-type blocks are aligned parallel to each other, and between them are rows of alkali metal ions. $CsBi_{3.67}Se_6$ consists of narrower NaCl-type infinite rods, which share edges. The cesium metal ions reside in the space between these rods. The bismuth sites that connect the NaCl-type rods are partially occupied. The $[Bi_2Se_4]^{2-}$ framework in $BaBi_2Se_4$ contains tunnels running along the c-axis that are occupied by Ba atoms. All compounds are narrow band-gap semiconductors. Electrical conductivity and thermoelectric power measurements show that **I**−**IV** exhibit n-type charge transport. Compounds **I** and **II**, however, can also exhibit p-type behavior. The thermal conductivity for **I** and **IV** is low with room-temperature values of ∼1.6 W/(m·K) for **I** and ∼1.2 W/(m·K) for **IV**. The optical band gaps of all compounds range between 0.3 and 0.6 eV.

Introduction

During the past decade a rich chemistry associated with ternary and quaternary bismuth chalcogenides has emerged that rivals in diversity and attractiveness that of the complex mineral bismuth sulfosalts. This revival in the chemistry of bismuth chalcogenides has resulted in the discovery of several new interesting ternary and quaternary compounds. Our group has contributed β-,γ-$CsBiS_2$,[1] KBi_3S_5,[2] $KBi_{6.33}S_{10}$,[3] $K_2Bi_8S_{13}$,[3] α-,β-$K_2Bi_8Se_{13}$,[1,4] $K_{2.5}Bi_{8.5}Se_{14}$,[4] $A_xBi_4Se_7$[5] (x = 1, 2), $BaBiTe_3$,[6] $CsBi_4Te_6$,[7] $ALn_{1\pm x}Bi_{4\pm x}S_8$[8] (A = K, Rb; Ln = La, Ce, Pr, Nd), $BaLaBi_2Q_6$[9] (Q = S, Se), α-,β-$APbBi_3Se_6$[10] (A = K, Rb, Cs), $K_{1-x}Sn_{5-x}Bi_{11+x}Se_{22}$,[11] and $A_{1+x}M'_{4-2x}Bi_{7+x}Se_{15}$[12] (A = K, Rb; M′ = Sn, Pb). Other groups have described $Sn_4Bi_2Se_7$,[13] $SnBi_4Se_7$,[14] $CdBi_2S_4$,[15] $CdBi_4S_7$,[15]

† Department of Chemistry and Center for Fundamental Materials Research, Michigan State University.
‡ Northwestern University.
§ University of Michigan.
|| Department of Electrical and Computer Engineering.

(1) McCarthy, T. J.; Ngeyi, S.-P.; Liao, J.-H.; DeGroot, D.; Hogan, T.; Kannewurf, C. R.; Kanatzidis, M. G. *Chem. Mater.* **1993**, *5*, 331−340.
(2) McCarthy, T. J.; Tanzer, T. A.; Kanatzidis, M. G. *J. Am. Chem. Soc.* **1995**, *117*, 1294−1301.
(3) Kanatzidis, M. G.; McCarthy, T. J.; Tanzer, T. A.; Chen, L.-H.; Iordanidis, L.; Hogan, T.; Kannewurf, C. R.; Uher, C.; Chen, B. *Chem. Mater.* **1996**, *8*, 1465−1474. (b) Chen, B.; Uher, C.; Iordanidis, L.; Kanatzidis, M. G. *Chem. Mater.* **1997**, *9*, 1655−1658.
(4) Chung, D.-Y.; Choi, K.-S.; Iordanidis, L.; Kanatzidis, M. G.; Schindler, J. L.; Brazis, P. W.; Kannewurf, C. R.; Chen, B.; Hu, S.; Uher, C. *Chem. Mater.* **1997**, *9* 3060−3071.
(5) Iordanidis, L.; Kanatzidis, M. G. *Angew. Chem., Int. Ed. Engl.* **2000**, *39*, 1927−1930.
(6) Chung, D.-Y.; Jobic, S.; Hogan, T.; Kannewurf, C. R.; Brec, R.; Rouxel, R.; Kanatzidis, M. G. *J. Am. Chem. Soc.* **1997**, *119*, 2505−2515.
(7) Chung, D.-Y.; Hogan, T.; Brazis, P. W.; Kannewurf, C. R.; Bastea, M.; Uher, C.; Kanatzidis, M. G. *Science* **2000,** *287*, 1024−1027.
(8) Iordanidis, L.; Schindler, J. L.; Kannewurf, C. R.; Kanatzidis, M. G. *J. Solid State Chem.* **1999**, *143* (2), 151−162.
(9) Choi, K.-S.; Iordanidis, L.; Chondroudis, K.; Kanatzidis, M. G. *Inorg. Chem.* **1997**, *36*, 3804−3805.
(10) Chung, D.-Y.; Iordanidis, L.; Rangan, K. K.; Brazis, P. W.; Kannewurf, C. R.; Kanatzidis, M. G. *Chem. Mater.* **1999**, *11*, 1352−1362.
(11) Mroztek, A.; Chung, D.-Y.; Hogan, T.; Kanatzidis, M. G. *J. Mater. Chem.* **2000**, *10*, 1667−1672.
(12) Choi, K.-S.; Chung, D.-Y.; Mroztek, A.; Brazis, P. W.; Kannewurf, C. R.; Kanatzidis, M. G. *Chem. Mater.*, in press.

10.1021/cm000734a CCC: $20.00
Published on Web 01/17/2001

$Cd_{2.8}Bi_{8.1}S_{15}$,[15] $Cd_2Bi_6S_{11}$,[15] $Ba_3Bi_{6.67}Se_{13}$,[16] and $Ba_3MBi_6Se_{13}$[16] (M = Sn, Pb). Prior to these developments only a few bismuth chalcogenides were known such as $ABiQ_2$ (A = alkali metal; Q = chalcogen),[17] $CsBi_3S_5$,[18] $RbBi_3S_5$,[19] $Cs_3Bi_7Se_{12}$,[20] α-,β-$BaBi_2S_4$,[21] $SrBiSe_3$,[22] $Sr_4Bi_6Se_{13}$,[23] and $BaBiSe_3$.[24]

Substantial interest in this class of compounds derives from their potential as thermoelectric materials. Our work has shown that these types of compounds can possess low thermal conductivity, high thermopower, and often high electrical conductivity,[25] reaching in the case of $CsBi_4Te_6$, a *ZT* [26] of 0.8 at 225 K. This value is comparable to those of the best $Bi_{2-x}Sb_xTe_{3-y}Se_y$[27] alloys currently used in thermoelectric applications.

From a solid-state chemistry perspective, bismuth chalcogenides are a fascinating class of compounds with staggering compositional and structural complexity.[28] These characteristics are spectacularly expressed in the natural occurring sulfosalts where Bi compounds are well represented. The stereochemical activity of the $6s^2$ lone pair causes bismuth to adopt several different coordination geometries depending on composition. When the lone pair is suppressed by hybridizing with energetically adjacent p and d orbitals, bismuth atoms adopt a normal octahedral geometry with six almost equidistant Bi−Q bonds and angles around 90°. This is not observed very often however, and usually the bismuth atoms adopt distorted octahedral geometries having short bonds trans to long bonds and resulting in coordination environments that resemble a trigonal pyramid, a square pyramid, or a trigonal bipyramid. Furthermore, this astonishing bonding flexibility of bismuth enables it to occupy sites with coordination numbers up to 9 and, when possible, to participate in mixed site occupation with similarly sized atoms, e.g. Pb, Sn, lanthanide, alkali metal, or alkaline earth metal atoms.

When combined together by sharing edges, the Bi−Q octahedra form blocks that derive from the NaCl-, Bi_2Te_3-, CdI_2-, and Sb_2Se_3-type structures. These octahedral blocks come in different shapes and sizes and are usually connected either directly with each other or through metal atoms of high (>6) coordination. These characteristics point to a seemingly countless number of novel phases that can potentially form.

The features mentioned above can generate complexity, diversity, and disorder that are desirable in good thermoelectric materials because they can lead to corresponding complexities in electronic structure as well as low thermal conductivity.[29,30] For example, β-$K_2Bi_8Se_{13}$ shows promising thermoelectric properties by virtue of its very low thermal conductivity and relatively high power factor.[4,26] Doping studies on this system have shown that its *ZT* can be substantially improved.[4,31,44] We report here the synthesis, physicochemical, spectroscopic, and structural characterization of four new compounds, $Rb_2Bi_8Se_{13}$, $Cs_2Bi_8Se_{13}$, $CsBi_{3.67}Se_6$, and $BaBi_2Se_4$. The $A_2Bi_8Se_{13}$ (A = Rb, Cs) compounds feature a novel structure type. Electrical conductivity, thermopower, and thermal conductivity measurements on selected systems are also reported.

Experimental Section

Reagents. Chemicals were used as obtained: bismuth powder (99.999+%, −100 mesh, Cerac, Milwaukee, WI); bismuth chunks (99.999% Noranda, Toronto, Canada); selenium powder (99.95% purity, −200 mesh, Cerac Inc., Milwaukee); selenium shots (99.999% Noranda, Toronto, Canada); bismuth selenide powder (99.999% purity, −325 mesh, Cerac Inc., Milwaukee, WI); rubidium metal (99.8% purity, Alfa Aesar, Ward Hill, MA); cesium metal (99.98% purity, Alfa Aesar, Ward Hill, MA); barium selenide powder (99.5% purity, −20 mesh, Cerac Inc., Milwaukee, WI). A_2Se (A = Rb, Cs) was prepared by a stoichiometric reaction of the corresponding alkali metal and selenium in liquid ammonia.

Synthesis. All manipulations were carried out under a dry nitrogen atmosphere in a Vacuum Atmospheres Dri-Lab glovebox. All products were washed with degassed methanol and ether to remove any traces of excess flux. For all compounds the yield was almost quantitative (∼100%) and the purity and homogeneity of the products was verified by comparing the X-ray powder diffraction patterns to those calculated by the crystallographically determined atomic coordinates.

Bi_2Se_3. A mixture of 9.407 g (0.045 mol) of Bi and 5.331 g (0.068 mol) of Se was transferred into a silica tube, which was

(13) Adouby, K.; Perez Vicente, C.; Jumas, J. C.; Fourcade, R.; Abba Touré, A. *Z. Kristallogr.* **1998**, *213*, 343−349.

(14) Perez Vicente, C.; Tirado, J. L.; Adouby, K.; Jumas, J. C.; Abba Touré, A.; Kra, G. *Inorg. Chem.* **1999**, *38*, 2131−2135.

(15) Choe, W.; Lee, S.; O'Connell, P.; Covey A. *Chem. Mater.* **1997**, *9*, 2025−2030.

(16) Wang, Y. C.; DiSalvo, F. J. *Chem. Mater.* **2000**, *12*, 1011−1017.

(17) Boon, J. W. *Recl. Trav. Chim. Pays-Bas* **1944**, *63*, 32. (b) Glemser, O.; Filcek, M. *Z. Anorg. Allg. Chem.* **1955**, *279*, 321−323. (c) Gattow, G.; Zemann, J. *Z. Anorg. Allg. Chem.* **1955**, *279*, 324−327. (d) Voroshilov, Y. V.; Peresh, E. Y.; Golovei, M. I. *Inorg. Mater.* **1972**, *8*, 677−678.

(18) Kanischeva, A. S.; Mikhailov, J. N.; Lasarev, V. B.; Trippel, A. F. *Dokl. Akad. Nauk., SSSR (Kryst.)* **1980**, *252*, 96−99.

(19) Schmitz, D.; Bronger, W. *Z. Naturforsch.* **1974**, *29b*, 438−439.

(20) Cordier, G.; Schäfer, H.; Schwidetzky, C. *Rev. Chim. Miner.* **1985**, *22*, 676−683.

(21) Aurivillus, B. *Acta Chem. Scand.* **1983**, *A37*, 399−407.

(22) Cook, R.; Schäfer, H. *Rev. Chim. Miner.* **1982**, *19*, 19−27.

(23) Cordier, G.; Schäfer, H.; Schwidetzky, C. *Rev. Chim. Miner.* **1985**, *22*, 631−638.

(24) Volk, K.; Cordier, G.; Cook, R.; Schäfer, H. *Z. Naturforsch.* **1980**, *35b*, 136−140.

(25) Kanatzidis, M. G.; McCarthy, T. J.; Tanzer, T. A.; Chen, L.-H.; Hogan, T.; Kannewurf, C. R.; Iordanidis, L. *Mater. Res. Soc. Symp. Proc.* **1996**, *410*, 37−43. (b) Chung, D-.Y.; Hogan, T.; Schindler, J. L.; Iordanidis, L.; Brazis, P. W.; Kannewurf, C. R.; Chen, B.; Uher, C.; Kanatzidis, M. G. *Mater. Res. Soc. Symp. Proc.* **1997**, *478*, 333−344. (c) Iordanidis, L.; Brazis, P. W.; Kannewurf, C. R.; Kanatzidis, M. G. *Mater. Res. Soc. Symp. Proc.* **1999**, *545*, 189−196. (d) Kanatzidis, M. G.; Chung, D-.Y.; Iordanidis, L.; Choi, K.-S.; Brazis, P. W.; Hogan, T.; Kannewurf, C. R. *Mater. Res. Soc. Symp. Proc.* **1999**, *545*, 233−246.

(26) The thermoelectric figure of merit is defined as $ZT = (S^2\sigma/\kappa)T$, where *S* is the thermopower, σ the electrical conductivity, κ the thermal conductivity, and *T* the temperature. The numerator $S^2\sigma$ is called the power factor. All three of these properties are determined by the details of the electronic structure and scattering of charge carriers (electrons or holes) and thus are not independently controllable parameters. κ also has a contribution from lattice vibrations, κ_l, the phonon thermal conductivity. Thus $\kappa = \kappa_e + \kappa_l$, where κ_e is the electronic thermal conductivity.

(27) *CRC Handbook of Thermoelectrics*; Rowe, D. M., Ed.; CRC Press: Boca Raton, FL, 1995; and references therein.

(28) Makovicky, E. *Fortschr. Miner.* **1981**, *59*, 137−190. (b) Makovicky, E. *Fortschr. Miner.* **1985**, *63*, 45−89. (c) Makovicky, E. *Z. Kristallogr.* **1985**, *173*, 1−23. (d) Makovicky, E. *Neues Jahrb. Mineral. Abh.* **1989**, *160*, 269−297. (e) Makovicky, E. *Eur. J. Mineral.* **1993**, *5*, 545−591.

(29) Chung, D.-Y.; Iordanidis, L.; Choi, K.-S.; Kanatzidis, M. G. *Bull. Kor. Soc.* **1998**, *19*, 1283−1293. (b) Kanatzidis, M. G. *Semicond. Semimet.* **2000**, *69*, 51−100.

(30) Slack, G. A. New Materials and Performance Limits for Thermoelectric Cooling. In *CRC Handbook of Thermoelectrics*; Rowe, D. M., Ed.; CRC Press: Boca Raton, FL, 1995; pp 407−440. (b) Slack, G. A. In *Solid State Physics*; Ehrenreich, H., Seitz, F., Turnbull, D., Eds.; Academic Press: New York, 1997; Vol. 34, p 1.

(31) Brazis, P. W.; Ireland, J. R.; Lane, M. A.; Kyratsi, T.; Chung, D.-Y.; Kanatzidis, M. G.; Kannewurf, C. R. *Mater. Res. Soc. Symp Proc.* **2000**, in press.

flame-sealed under vacuum. The tube was heated to 600 °C in 12 h, held at 600 °C for 2 d, and then cooled to 50 °C in 6 h. The product was pulverized and used for further reactions.

$Rb_2Bi_8Se_{13}$ (I). A mixture of 0.065 g (0.260 mmol) of Rb_2Se and 0.568 g (0.867 mmol) of Bi_2Se_3 was transferred to a carbon-coated silica tube and was flame-sealed under vacuum. The tube was heated for 2.5 d at 750 °C and then cooled to 50 °C in 12 h. The product consisted of silvery-gray thin needlelike crystals. Semiquantitative energy dispersive analysis (EDS) using a scanning electron microscope (SEM) on several needles gave an average composition of $Rb_{2.6}Bi_{7.9}Se_{13}$.

$Cs_2Bi_8Se_{13}$ (II). A mixture of 0.065 g (0.188 mmol) of Cs_2Se and 0.412 g (0.629 mmol) of Bi_2Se_3 was transferred to a carbon-coated silica tube and was flame-sealed under vacuum. The tube was heated the same as for the case of **I**. The product was obtained as silvery-gray thin needlelike crystals. SEM/EDS analysis on several crystals gave an average composition of $Cs_{2.2}Bi_{7.9}Se_{13}$.

$CsBi_{3.67}Se_6$ (III). *Method I***.** Initially $CsBi_{3.67}Se_6$ was synthesized as follows: A mixture of 0.065 g (0.189 mmol) of Cs_2Se, 0.242 g (0.904 mmol) of Bi, and 0.138 g (1.747 mmol) of Se was transferred to a carbon-coated silica tube which was flame-sealed under vacuum. The tube was heated for 6 d at 750 °C and then cooled to 50 °C at 10 °C/h. The product consisted of silvery-gray polycrystalline rods.

*Method II***.** A mixture of 0.130 g (0.337 mmol) of Cs_2Se and 0.824 g (1.258 mmol) of Bi_2Se_3 was transferred to a silica tube which was flame-sealed under vacuum. The tube was placed under the flame of a natural gas−oxygen torch until the mixture melted, and then the tube was removed from the flame and let to solidify. The procedure was repeated two more times to ensure homogeneity. The product consisted of a silvery chunk with needles growing across its surface. SEM/EDS analysis on several crystals gave an average composition of $Cs_{1.2}Bi_{3.7}Se_6$.

$BaBi_2Se_4$ (IV). A mixture of 0.050 g (0.231 mmol) of BaSe and 0.151 g (0.231 mmol) of Bi_2Se_3 was transferred to a carbon-coated silica tube, which was flame-sealed under vacuum. The tube was heated for 3 d at 750 °C, cooled to 450 °C at 30 °C/h, and further cooled to 50 °C in 6 h. The product consisted of polycrystalline silvery chunks. SEM/EDS analysis on several crystals gave an average composition of $Ba_{1.2}Bi_{1.9}Se_4$.

Physical Measurements

Electron Microscopy. Quantitative microprobe analyses of the compounds were performed with a JEOL JSM-6400V scanning electron microscope equipped with either a Noran TN-5500 or a Noran Vantage energy dispersive spectroscopy detector. Data were collected for 45 s using an accelerating voltage of 25 kV.

Differential Thermal Analysis. Differential thermal analysis (DTA) was performed with a computer-controlled thermal analyzer (Shimadzu DTA-50). Ground single crystals (20−50 mg) were sealed in silica ampules under vacuum. A silica ampule containing alumina of equal mass was sealed and placed on the reference side of the detector. The samples were heated to the desired temperature at 10 °C/min, isothermed for 5 min, and then cooled at 10 °C/min. The reported DTA temperature is the peak temperature upon heating. After DTA, the samples were examined with powder X-ray diffraction.

Infrared Spectroscopy. Optical band gaps were determined from diffuse reflectance measurements made on the finely ground sample at room temperature. The spectra were recorded in the infrared region (6000−400 cm^{-1}) with a Nicolet MAGNA-IR 750 spectrometer equipped with a diffuse reflectance attachment from Spectra-Tech. Inc. Absorption (α/S) data were calculated from the reflectance data using the Kubelka−Munk function.[32] The band gap was defined as the intersection point between energy axis at the absorption offset and the line extrapolated from the linear portion of the absorption edge in a α/S vs E (eV) plot.

Charge-Transport and Thermal Conductivity Measurements. At Northwestern University dc electrical conductivity and thermopower measurements were made on single crystals and polycrystalline aggregates of the compound. Conductivity measurements were performed in the usual four-probe geometry with 60- and 25-μm gold wires used for the current and voltage electrodes, respectively. Measurements of the sample cross-sectional area and voltage probe separation were made with a calibrated binocular microscope. Conductivity data were obtained with the computer-automated system described elsewhere.[33a] Thermoelectric power measurements were made by using a slow ac technique[33b] with 10-μm gold wires serving to support and conduct heat to the sample, as well as to measure the voltage across the sample resulting from the applied temperature gradient. In both measurements, the gold electrodes were attached on the samples with a conductive gold paste. The temperature drift rate during an experiment was kept below 1 K/min. Typically, three to four separate variable-temperature runs were carried out for each sample to ensure reproducibility and stability. At a given temperature, reproducibility was within ±1%.

At the University of Michigan electrical resistivity was measured using a Linear Research AC bridge with 16 Hz excitation in a cryostat equipped with a magnet capable of fields up to 5.5 T. Thermal conductivity and thermopower were determined using a longitudinal steady-state method over the temperature range 4−300 K. In this case samples were attached (using either a low melting point solder or silver-loaded epoxy) to the cold tip of the cryostat, while the other end of the sample is provided with a small strain gauge resistor (thin film) which serves as a heater. Temperature difference across the sample is measured using a differential chromel−constantan thermocouple. The Seebeck voltage was measured with thin copper wire the thermopower of which was calibrated against a high-T_c superconductor up to 134 K.

At Michigan State University a four sample measurement system was used to measure simultaneously electrical conductivity, thermoelectric power, and thermal conductivity.[34] To fully characterize the figure of merit, the properties were measured for each sample over the selective temperature range of interest (system capability is 4.2−475 K). To alleviate offset error voltages and increase the density of data points, a slow-ac technique was used with a heater pulse period of 720 s.[35] The pulse shape was monitored, in situ, to determine temperature stabilization, and the sample chamber was maintained at a pressure less than 10^{-5} Torr for the entire measurement run. Samples were mounted in the standard four probe configuration for the thermal conductivity, and the heater current was adjusted for an average temperature gradient of 1 K. The sample stage and radiation shield were gold-coated copper to minimize radiation effects and to maintain temperature uniformity. All electrical leads were 25 μm in diameter with lengths greater than 10 cm to minimize thermal conduction losses. Data acquisition and computer control of the system was maintained under the LabVIEW[36] software environment.

Powder X-ray Diffraction. The compounds were examined by X-ray powder diffraction to assess phase purity and for identification. Powder patterns were obtained using a Rigaku-Denki/Rw400F2 (Rotaflex) rotating-anode powder diffractometer and a CPS 120 INEL X-ray powder diffractometer equipped with a position-sensitive detector. The purity and homogeneity of all phases was confirmed by comparison of

(32) Wendlandt, W. W.; Hecht, H. G. *Reflectance Spectroscopy*; Interscience Publishers: New York, 1966. (b) Kotüm, G. *Reflectance Spectroscopy*; Springer-Verlag: New York, 1969. (c) Tandon, S. P.; Gupta, J. P. *Phys. Status Solidi* **1970**, *38*, 363−367.

(33) Lyding, J. W.; Marcy, H. O.; Marks, T. J.; Kannewurf, C. R. *IEEE Trans. Instrum. Meas.* **1988**, *37*, 76−80. (b) Marcy, H. O.; Marks, T. J.; Kannewurf, C. R. *IEEE Trans. Instrum. Meas.* **1990**, *39*, 756−760.

(34) Hogan, T.; Ghelani, N.; Loo, S.; Sportouch, S.; Kim, S.-J.; Chung, D.-Y.; Kanatzidis, M. G. *Proc. Int. Conf. Thermoelectr.* **1999,** 671−674.

(35) Maldonado, O. *Cryogenics* **1992**, *32*, 908−912.

(36) LabVIEW, Version 5.0, National Instruments, Austin, TX, 1999.

Table 1. Crystallographic Data for $A_2Bi_8Se_{13}$ (A = Rb, Cs), $CsBi_{3.67}Se_6$, and $BaBi_2Se_4$

empirical formula	$Rb_2Bi_8Se_{13}$ (**I**)	$Cs_2Bi_8Se_{13}$ (**II**)	$CsBi_{3.67}Se_6$ (**III**)	$BaBi_2Se_4$ (**IV**)
fw	2869.26	2964.14	1372.58	880.98
temp, K	173.1(1)	173.1(1)	296(2)	173.1(1)
cryst system	monoclinic	monoclinic	orthorhombic	hexagonal
space group	$P2_1/m$	$P2_1/m$	$Pnma$	$P6_3/m$
unit cell dimens, Å, deg	a = 13.4931(4)	a = 13.704(1)	a = 23.421(4)	a = 26.157(1)
	b = 4.1558(3)	b = 4.1532(4)	b = 4.1877(8)	b = 26.157(1)
	c = 24.876(2)	c = 25.008(2)	c = 13.710(3)	c = 4.3245(3)
	β = 96.571(4)	β = 96.848(2)		γ =120
Z; V, Å^3	2, 1385.78(1)	2, 1413.2(2)	4, 1344.7(4)	12, 2562.4(3)
D(calcd), g/cm^3	6.876	6.966	6.780	6.851
abs coeff, mm^{-1}	71.156	68.892	66.680	62.932
F(000)	2360	2432	2253	4334
cryst size, mm^3	0.40 × 0.03 × 0.02	0.02 × 0.02 × 0.30	0.03 × 0.03 × 0.44	0.02 × 0.03 × 0.30
θ range for data collcn, deg	1.52−28.75	1.62−25.99	1.72−26.37	3.60−30.68
index ranges	$-17 \le h \le 17$	$-16 \le h \le 16$	$-29 \le h \le 28$	$-35 \le h \le 37$
	$-5 \le k \le 5$	$-5 \le k \le 4$	$-5 \le k \le 5$	$-35 \le k \le 36$
	$-32 \le l \le 32$	$-30 \le l \le 19$	$-16 \le l \le 17$	$-6 \le l \le 6$
reflcns collcd	10 652	8004	10 914	29 993
indepdt reflcns	3680 [R(int) = 0.1065]	3155 [R(int) = 0.0541]	1565 [R(int) = 0.1027]	2857 [R(int) = 0.0989]
refinement method	full-matrix least squares on F^2			
data/restraints/params	3680/0/140	3155/0/140	1565/0/68	2857/0/89
goodness-of-fit on F^2	0.914	0.969	1.053	1.088
final R indices [$I > 2\sigma(I)$]	R1 = 0.0577, wR2 = 0.1159	R1 = 0.0497, wR2 = 0.1123	R1 = 0.0611, wR2 = 0.1384	R1 = 0.0371, wR2 = 0.0817
R indices (all data)	R1 = 0.1164, wR2 = 0.1244	R1 = 0.0668, wR2 = 0.1167	R1 = 0.0737, wR2 = 0.1421	R1 = 0.0494, wR2 = 0.0850
extinction	0.000 144(18)	0.000 37(3)	0.001 96(18)	0.000 33(3)
largest peak and hole, e Å^{-3}	4.825 and 4.801	4.775 and 3.600	3.889 and 3.310	4.424 and 2.573

X-ray powder diffraction to those calculated from single-crystal data using the CERIUS^2 software.[37]

Single-Crystal X-ray Crystallography. A Bruker SMART Platform CCD diffractometer was used for data collection. Several different sets of frames covering a random area of the reciprocal space were collected using 0.3° steps in ω at a detector-to-sample distance of ~5 cm. The SMART software was used for data acquisition and SAINT[38] for data extraction. The absorption correction was done with SADABS,[38] and the structure solution and refinement was done with the SHELX-TL[38] package of crystallographic programs. All structures were solved with direct methods. All atoms were refined anisotropically.

$Rb_2Bi_8Se_{13}$ (I). Almost a full sphere of data was collected (1730 frames) with an exposure time of 35 s/frame. The final cell was calculated from 1550 [$I > 10\sigma(I)$] reflections selected from the entire data set (Table 1). The resolution of the data set was 0.74 Å. Eight bismuth atoms, two rubidium, and thirteen selenium atoms were found to sit on a crystallographic mirror plane. Final R values were R1 = 5.77% and wR2 = 11.59%. The fractional atomic coordinates and equivalent isotropic displacement parameters are shown in Table 2.

$Cs_2Bi_8Se_{13}$ (II). A hemisphere of data was collected (1324 frames) with an exposure time of 55 s/frame. The final cell was calculated from 4524 reflections [$I > 8\sigma(I)$] selected from the entire data set (Table 1). The resolution of the data set was 0.81 Å. Because the compound is isostructural with **I,** the fractional atomic coordinates from **I** were used to refine the structure. Final R values were R1 = 4.97% and wR2 = 11.23%. The fractional atomic coordinates and equivalent isotropic displacement parameters are shown in Table 3.

$CsBi_{3.67}Se_6$ (III). Almost a full sphere of data was collected (2047 frames) with an exposure time of 30 s/frame. The final cell was calculated from 2888 reflections [$I > 8\sigma(I)$] selected from the entire data set (Table 1). The resolution of the data set was 0.80 Å. Four bismuth atoms, one cesium, and six selenium atoms were found to sit on a crystallographic mirror plane. After refinement, the R1 and wR2 values were 11.2% and 29.2% respectively. At this point the U_{iso} of Bi(4) was 0.051 Å^2, high compared to the other three Bi atoms (average U_{iso} ~ 0.017 Å^2), and there was not enough negative charge in the structure $Cs^+[Bi_4Se_6]^0$. When the occupancy of Bi(4) was let to refine, it and the temperature factor dropped to 0.34/0.026 Å^2 respectively (R1 = 9.7%, wR2 = 22.4%). This occupancy value corresponds to 66% occupation, exactly what is needed for electroneutrality. Final R values were R1 = 6.11% and wR2 = 13.84%. The fractional atomic coordinates and equivalent isotropic displacement parameters are shown in Table 4.

$BaBi_2Se_4$ (IV). A full sphere of data was collected (2140 frames) with an exposure time of 60 s/frame. The final cell was calculated from 10191 reflections (Table 1). The resolution of the data set was 0.70 Å. Four Bi, two Ba, and nine Se atoms were found to sit on a crystallographic mirror plane. After refinement, the R1 and wR2 values were 7.8% and 19.8% respectively. At this point one of the nine selenium atoms was sitting in the center of a channel having distances to the neighboring Se atoms between 3.083(2) and 3.776(2) Å and generating a symmetry-equivalent atom 2.16 Å away. Therefore this atom was assigned as Ba(3) and its occupancy was refined (R1 = 5.8%, wR2 = 16.8%). The occupancy of Ba(3) was refined to 0.07266 (full occupancy 0.16667). Final R values

Table 2. Atomic Coordinates and Equivalent Isotropic Displacement Parameters (Å^2 × 10^3) for $Rb_2Bi_8Se_{13}$

	x	y	z	U_{eq}[a]
Bi(1)	0.0520(1)	−0.7500	0.4411(1)	13(1)
Bi(2)	−0.1280(1)	−0.7500	0.2130(1)	10(1)
Bi(3)	0.2802(1)	−0.2500	0.0320(1)	11(1)
Bi(4)	0.4387(1)	−0.2500	0.2674(1)	10(1)
Bi(5)	0.1158(1)	−0.2500	0.3084(1)	12(1)
Bi(6)	−0.0488(1)	−0.2500	0.0708(1)	12(1)
Bi(7)	0.1943(1)	0.2500	0.1708(1)	12(1)
Bi(8)	0.4249(1)	−0.7500	0.4357(1)	15(1)
Rb(1)	−0.2750(3)	−0.7500	0.3618(1)	19(1)
Rb(2)	0.5829(3)	−0.2500	0.1187(1)	21(1)
Se(1)	−0.1027(3)	−0.2500	0.4489(1)	13(1)
Se(2)	0.1965(3)	−0.2500	0.4154(1)	13(1)
Se(3)	−0.0304(3)	−0.7500	0.3208(1)	12(1)
Se(4)	0.0370(3)	−0.2500	0.1832(1)	9(1)
Se(5)	−0.2517(3)	−0.2500	0.2369(1)	14(1)
Se(6)	−0.1930(3)	−0.7500	0.0891(1)	13(1)
Se(7)	0.1037(3)	0.2500	0.0494(1)	9(1)
Se(8)	0.4126(3)	−0.7500	0.0216(1)	11(1)
Se(9)	0.3297(3)	−0.2500	0.1461(1)	10(1)
Se(10)	0.2616(3)	0.2500	0.2828(1)	11(1)
Se(11)	0.5582(3)	−0.7500	0.2385(1)	10(1)
Se(12)	0.5188(3)	−0.2500	0.3725(1)	12(1)
Se(13)	0.6129(3)	−0.7500	0.4864(1)	10(1)

[a] U_{eq} is defined as one-third of the trace of the orthogonalized $\mathbf{U}_{ij}$ tensor.

(37) CERIUS^2, Version 3.8., Molecular Simulations Inc., Cambridge, England, 1999.

(38) SMART v4 and v5, 1996−1999, SAINT v4, v5, and v6, 1994−1999, SADABS, SHELXTL V-5, Bruker Analytical Xray Systems Inc., Madison, WI 53719.

Table 3. Atomic Coordinates and Equivalent Isotropic Displacement Parameters (Å^2 × 10^3) for $Cs_2Bi_8Se_{13}$

	x	*y*	*z*	U_{eq}[a]
Bi(1)	0.0528(1)	−0.7500	0.4410(1)	15(1)
Bi(2)	−0.0251(1)	−0.7500	0.2132(1)	13(1)
Bi(3)	0.2764(1)	−0.2500	0.0329(1)	13(1)
Bi(4)	0.4357(1)	−0.2500	0.2673(1)	13(1)
Bi(5)	0.1178(1)	−0.2500	0.3087(1)	14(1)
Bi(6)	−0.0477(1)	−0.2500	0.0706(1)	14(1)
Bi(7)	0.1915(1)	0.2500	0.1706(1)	14(1)
Bi(8)	0.4238(1)	−0.7500	0.4363(1)	17(1)
Cs(1)	−0.2739(1)	−0.7500	0.3621(1)	18(1)
Cs(2)	0.5824(1)	−0.2500	0.1183(1)	20(1)
Se(1)	−0.0993(2)	−0.2500	0.4496(1)	15(1)
Se(2)	0.1953(2)	−0.2500	0.4154(1)	15(1)
Se(3)	−0.0269(2)	−0.7500	0.3201(1)	13(1)
Se(4)	0.0366(2)	−0.2500	0.1833(1)	13(1)
Se(5)	−0.2464(2)	−0.2500	0.2369(1)	14(1)
Se(6)	−0.1885(2)	−0.7500	0.0885(1)	14(1)
Se(7)	0.1031(2)	0.2500	0.0491(1)	13(1)
Se(8)	0.4072(2)	−0.7500	0.0233(1)	14(1)
Se(9)	0.3245(2)	−0.2500	0.1464(1)	13(1)
Se(10)	0.2606(2)	0.2500	0.2819(1)	13(1)
Se(11)	0.5540(2)	−0.7500	0.2396(1)	14(1)
Se(12)	0.5111(2)	−0.2500	0.3724(1)	14(1)
Se(13)	0.6100(2)	−0.7500	0.4857(1)	14(1)

[a] U_{eq} is defined as one-third of the trace of the orthogonalized $\mathbf{U}_{ij}$ tensor.

Table 4. Atomic Coordinates and Equivalent Isotropic Displacement Parameters (Å^2 × 10^3) for $CsBi_{3.67}Se_6$

	x	*y*	*z*	U_{eq}[a]	occ
Bi(1)	0.0763(1)	0.2500	0.5468(1)	20(1)	
Bi(2)	0.3253(1)	−0.7500	0.8336(1)	27(1)	
Bi(3)	0.0242(1)	−0.7500	0.2261(1)	24(1)	
Bi(4)	0.2162(1)	−0.2500	0.6558(1)	28(1)	0.67
Cs	0.1334(1)	−0.2500	−0.0370(1)	32(1)	
Se(1)	0.0461(1)	−0.2500	0.3985(2)	16(1)	
Se(2)	0.0010(1)	−0.7500	−0.1001(2)	21(1)	
Se(3)	0.0962(1)	−0.2500	0.6900(2)	18(1)	
Se(4)	0.3504(1)	−0.2500	0.6866(2)	23(1)	
Se(5)	0.1966(1)	0.2500	0.4858(2)	21(1)	
Se(6)	0.2120(1)	−0.7500	0.7875(2)	29(1)	

[a] U_{eq} is defined as one-third of the trace of the orthogonalized $\mathbf{U}_{ij}$ tensor.

were R1 = 3.71% and wR2 = 8.17%. The U_{33} of Ba(3) and the U_{11} of Se(7) were considerably higher than those of the other atoms and the formula was $Ba_{1.07}Bi_2Se_4$ indicating that there was 0.14 net positive charge per formula. Attempts to refine the occupancy of the other metal sites did not reveal any vacancies. Nevertheless, we believe that the extra charge must be distributed as vacancies throughout the metal sublattice and the very small fraction corresponding to each atom makes it very difficult to detect them by X-ray crystallography. Several other space groups were tried including $P\bar{3}$ and $P1$, but the behavior of Ba(3) and Se(7) was unchanged, with the Ba(3) atoms having large temperature factors in the direction of the tunnels and the Se(7) atoms having large temperature factors perpendicular to the tunnels toward the Ba(3) atom. Data were collected from a second crystal with identical results. The fractional atomic coordinates and equivalent isotropic displacement parameters are shown in Table 5.

Table 5. Atomic Coordinates and Equivalent Isotropic Displacement Parameters (Å^2 × 10^3) for $BaBi_2Se_4$

	x	*y*	*z*	U_{eq}[a]	occ
Bi(1)	0.4115(1)	0.4603(1)	0.2500	11(1)	
Bi(2)	0.5048(1)	0.6494(1)	-0.7500	10(1)	
Bi(3)	0.3333(1)	0.2743(1)	-0.7500	10(1)	
Bi(4)	0.1810(1)	0.1552(1)	-0.2500	14(1)	
Ba(1)	0.3243(1)	0.5552(1)	-0.2500	9(1)	
Ba(2)	0.2304(1)	0.3496(1)	-0.2500	9(1)	
Ba(3)	0.0000	0.0000	-0.2500	50(2)	0.436(9)
Se(1)	0.3048(1)	0.4533(1)	0.2500	9(1)	
Se(2)	0.3691(1)	0.3653(1)	-0.2500	10(1)	
Se(3)	0.4577(1)	0.5466(1)	-0.2500	11(1)	
Se(4)	0.4075(1)	0.6579(1)	-0.7500	9(1)	
Se(5)	0.5517(1)	0.7294(1)	-0.2500	9(1)	
Se(6)	0.3074(1)	0.1895(1)	-0.2500	10(1)	
Se(7)	0.1360(1)	0.0726(1)	-0.7500	34(1)	
Se(8)	0.2158(1)	0.2477(1)	-0.7500	11(1)	

[a] U_{eq} is defined as one-third of the trace of the orthogonalized $\mathbf{U}_{ij}$ tensor.

Results and Discussion

Synthesis and Thermal Behavior. $Rb_2Bi_8Se_{13}$ and $Cs_2Bi_8Se_{13}$ form by reacting almost stoichiometric (A_2Se:Bi_2Se_3 = 1.2:4) combinations of A_2Se (A = Rb, Cs) and Bi_2Se_3 at 750 °C for 2 days. The slight excess of A_2Se is needed to compensate for any loss occurring due to reaction with the silica tube. The Rb analogue of $CsBi_{3.67}Se_6$ could not be synthesized. Although $CsBi_{3.67}Se_6$ can be prepared from direct combination reactions, the product contains several impurities with $Cs_2Bi_8Se_{13}$ being the most significant. Pure $CsBi_{3.67}Se_6$ could only be synthesized by quenching a melt of the corresponding composition. $Rb_2Bi_8Se_{13}$ can be also prepared by stoichiometric melt quenching whereas $Cs_2Bi_8Se_{13}$ could only be synthesized by slow cooling in a furnace. Interestingly, quenching a mixture of nominal stoichiometry "$Cs_2Bi_8Se_{13}$" yielded a mixture of $CsBi_{3.67}Se_6$ and a new phase that is currently under investigation. Direct combination reactions in the furnace with lower A_2Se:Bi_2Se_3 ratios gave mixtures of $A_2Bi_8Se_{13}$ and Bi_2Se_3, whereas higher A_2Se:Bi_2Se_3 (A = Rb, Cs) ratios gave $A_2Bi_4Se_7$,[5] $A_3Bi_7Se_{12}$,[39a] and ABi_3Se_5.[39a]

$Rb_2Bi_8Se_{13}$ and $Cs_2Bi_8Se_{13}$ melt congruently at 673 and 664 °C, respectively. $CsBi_{3.67}Se_6$ melts at 686 °C, but it transforms to $Cs_2Bi_8Se_{13}$ as evidenced by powder X-ray diffraction.

Pure $BaBi_2Se_4$ was synthesized by reacting BaSe and Bi_2Se_3 at 1:1 ratio at 750 °C. Higher ratios in BaSe still give $BaBi_2Se_4$ while ratios rich in Bi_2Se_3 give $Ba_{4-x}Bi_{6+2/3x}Se_{13}$.[39] $BaBi_2Se_4$ can be also synthesized by quenching a melt with excess BaSe. $BaBi_2Se_4$ melts congruently at 846 °C.

Structure Description. *$A_2Bi_8Se_{13}$ (A = Rb, Cs).* $Rb_2Bi_8Se_{13}$ and $Cs_2Bi_8Se_{13}$ are analogues of $K_2Bi_8Se_{13}$. However, they adopt a different structure; see Figure 1. Since the Rb and Cs compounds are isomorphous, we will describe in detail only $Rb_2Bi_8Se_{13}$. The structure has a three-dimensional framework consisting of infinitely long rectangular NaCl-type rods running parallel to the *b*-axis. Similar building blocks with the same thickness but with different width are found in $CsBi_4Te_6$.[7] These rectangular rods are two Bi octahedra thick and three Bi octahedra wide (2 × 3). The blocks are connected through small CdI_2-type fragments and two Bi atoms in a square pyramidal coordination (Sb_2Se_3-type). The same feature with square pyramidal Bi atoms exists in α-$K_2Bi_8Se_{13}$,[1] which adopts a different structure type. As these rods are linked side by side they form parallel tunnels filled with rows of Rb^+ ions.

(39) Iordanidis, L.; Kanatzidis, M. G. Work in progress. (b) A compound with the formula $Ba_3Bi_{6.67}Se_{13}$ having the same structure type was reported recently; see ref 16.

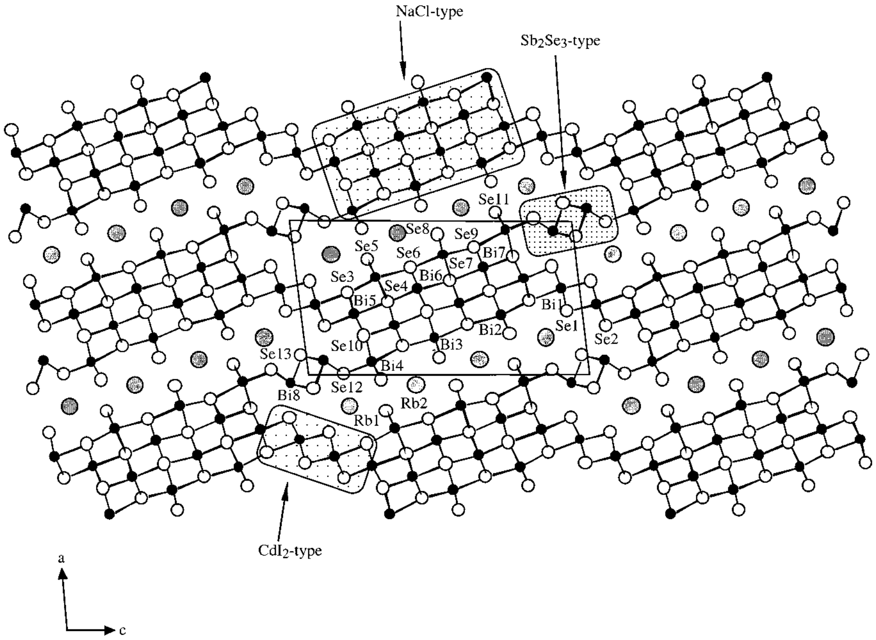

Figure 1. Projection of the structure of $A_2Bi_8Se_{13}$ down the *b*-axis. The shaded areas indicate the NaCl-, Sb_2Se_3- and CdI_2-type building blocks.

Table 6. Bond Distances (Å) for $A_2Bi_8Se_{13}$ (A = Rb, Cs)

$Rb_2Bi_8Se_{13}$		$Cs_2Bi_8Se_{13}$	
Bi(1)−Se(1)	2.745(4)	Bi(1)−Se(1)	2.736(3)
Bi(1)−Se(1)	2.968(3) × 2	Bi(1)−Se(1)	2.969(2) × 2
Bi(1)−Se(2)	2.968(3) × 2	Bi(1)−Se(2)	2.972(2) × 2
Bi(1)−Se(3)	3.070(4)	Bi(1)−Se(3)	3.088(3)
Bi(2)−Se(5)	2.771(3) × 2	Bi(2)−Se(5)	2.768(2) × 2
Bi(2)−Se(3)	2.849(4)	Bi(2)−Se(3)	2.848(3)
Bi(2)−Se(6)	3.108(4)	Bi(2)−Se(6)	3.134(3)
Bi(2)−Se(4)	3.195(3) × 2	Bi(2)−Se(4)	3.189(2) × 2
Bi(3)−Se(8)	2.772(3) × 2	Bi(3)−Se(8)	2.772(2) × 2
Bi(3)−Se(9)	2.840(4)	Bi(3)−Se(9)	2.837(3)
Bi(3)−Se(6)	3.106(4)	Bi(3)−Se(6)	3.131(3)
Bi(3)−Se(7)	3.226(3) × 2	Bi(3)−Se(7)	3.217(2) × 2
Bi(4)−Se(12)	2.714(4)	Bi(4)−Se(12)	2.706(3)
Bi(4)−Se(11)	2.775(3) × 2	Bi(4)−Se(11)	2.773(2) × 2
Bi(4)−Se(9)	3.202(4)	Bi(4)−Se(9)	3.220(3)
Bi(4)−Se(10)	3.222(3) × 2	Bi(4)−Se(10)	3.227(2) × 2
Bi(5)−Se(2)	2.758(4)	Bi(5)−Se(2)	2.753(3)
Bi(5)−Se(3)	2.907(3) × 2	Bi(5)−Se(3)	2.909(2) × 2
Bi(5)−Se(10)	2.980(3) × 2	Bi(5)−Se(10)	2.984(2) × 2
Bi(5)−Se(4)	3.174(3)	Bi(5)−Se(4)	3.198(3)
Bi(6)−Se(4)	2.900(3)	Bi(6)−Se(4)	2.917(3)
Bi(6)−Se(6)	2.918(3) × 2	Bi(6)−Se(6)	2.906(2) × 2
Bi(6)−Se(7)	2.997(3)	Bi(6)−Se(7)	2.999(3)
Bi(6)−Se(7)	3.014(3) × 2	Bi(6)−Se(7)	3.023(2) × 2
Bi(7)−Se(10)	2.830(4)	Bi(7)−Se(10)	2.830(3)
Bi(7)−Se(9)	2.879(3) × 2	Bi(7)−Se(9)	2.875(2) × 2
Bi(7)−Se(4)	3.012(3) × 2	Bi(7)−Se(4)	3.014(2) × 2
Bi(7)−Se(7)	3.125(4)	Bi(7)−Se(7)	3.133(3)
Bi(8)−Se(13)	2.700(4)	Bi(8)−Se(13)	2.700(3)
Bi(8)−Se(13)	2.927(2) × 2	Bi(8)−Se(13)	2.923(2) × 2
Bi(8)−Se(12)	2.974(3) × 2	Bi(8)−Se(12)	2.960(2) × 2
Bi(8)−Se(2)	3.704(3) × 2	Bi(8)−Se(2)	3.741(3) × 2
Rb(1)−Se(12)	3.507(4) × 2	Cs(1)−Se(12)	3.638(3) × 2
Rb(1)−Se(3)	3.563(5)	Cs(1)−Se(3)	3.661(3)
Rb(1)−Se(11)	3.592(5)	Cs(1)−Se(11)	3.636(4)
Rb(1)−Se(13)	3.600(5)	Cs(1)−Se(13)	3.641(3)
Rb(1)−Se(1)	3.641(4) × 2	Cs(1)−Se(1)	3.685(3) × 2
Rb(1)−Se(5)	3.782(4) × 2	Cs(1)−Se(5)	3.812(3) × 2
Rb(2)−Se(5)	3.481(5)	Cs(2)−Se(5)	3.556(4)
Rb(2)−Se(8)	3.499(5)	Cs(2)−Se(8)	3.561(3)
Rb(2)−Se(9)	3.559(5)	Cs(2)−Se(9)	3.685(3)
Rb(2)−Se(11)	3.678(4) × 2	Cs(2)−Se(11)	3.735(3) × 2
Rb(2)−Se(8)	3.764(4) × 2	Cs(2)−Se(8)	3.790(3) × 2
Rb(2)−Se(6)	3.810(4) × 2	Cs(2)−Se(6)	3.909(3) × 2

The Bi(8) atoms that exist in the Sb_2Se_3-type fragment mentioned above are five-coordinate, with a square pyramidal environment and Bi(8)−Se bond distances varying between 2.700(4) and 2.974(3) Å. There are also two other long Bi(8)−Se distances at 3.704(3) Å which are not considered bonding. All other Bi atoms in the structure have octahedral environments with varying degrees of distortion. Atom Bi(6), located in the center of the NaCl-type (2 × 3) block, is the least distorted atom with Bi(6)−Se distances between 2.900(3) and 3.014(3) Å and Se−Bi(6)−Se angles between 85.38(9) and 93.57(9)°. The other octahedral Bi atoms exhibit two different kinds of distortion. The first causes the octahedron to distort toward a square pyramid having four bonds, almost equal in length between 2.9 and 3.0 Å, one shorter one between 2.7 and 2.8 Å, and a longer one ≥3.1 Å trans to the shorter one. The second creates a trigonal pyramid with three short Bi−Se bonds opposite to three longer ones; see Table 6. The Bi(1), Bi(5), and Bi(7) octahedra are distorted toward a square pyramid; e.g., Bi(5) has four bonds between 2.907(3) and 2.980(3) Å, one bond at 2.758(4) Å, and one bond at 3.174(3) Å. The Bi(2), Bi(3), and Bi(4) octahedra are distorted toward a trigonal pyramid; e.g., Bi(4) has three short Bi−Se bonds between 2.714(4) and 2.775(3) Å and three longer ones between 3.202(4) and 3.222(3) Å.

The Rb^+ ions have a tricapped trigonal prismatic coordination with distances between 3.507(4) and 3.782(4) Å for Rb(1) and 3.481(5) and 3.810(4) Å for Rb(2). $Cs_2Bi_8Se_{13}$ has very similar characteristics and will not be discussed further. Selected bond distances and angles are shown in Tables 6 and 7.

As mentioned earlier, the structure of $A_2Bi_8Se_{13}$ (A = Rb, Cs) is different from those of α-,β-$K_2Bi_8Se_{13}$ although it has some similar features with α-$K_2Bi_8Se_{13}$. The structures of α-,β-$K_2Bi_8Se_{13}$ are shown in Figure 2. β-$K_2Bi_8Se_{13}$ consists of CdI_2-, NaCl-, and Bi_2Te_3-type fragments. $A_2Bi_8Se_{13}$ (A = Rb, Cs) does not contain Bi_2Te_3-type fragments, and its NaCl-type block is elongated in one direction compared with the NaCl-type block in β-$K_2Bi_8Se_{13}$ which has a neatly squarelike cross section. The connectivity of the blocks in the two structures is different, and as a result, the cavities

Table 7. Selected Angles (deg) for $A_2Bi_8Se_{13}$ (A = Rb, Cs)

$Rb_2Bi_8Se_{13}$		$Cs_2Bi_8Se_{13}$	
Se(1)−Bi(1)−Se(3)	83.35(9)	Se(1)−Bi(1)−Se(3)	84.33(7)
Se(1)−Bi(1)−Se(2)	90.46(7)	Se(1)−Bi(1)−Se(2)	90.69(5)
Se(1)−Bi(1)−Se(2)	96.92(9)	Se(1)−Bi(1)−Se(2)	97.74(7)
Se(1)−Bi(1)−Se(3)	173.2(1)	Se(1)−Bi(1)−Se(3)	172.78(8)
Se(4)−Bi(2)−Se(4)	81.14(8)	Se(4)−Bi(2)−Se(4)	81.26(6)
Se(5)−Bi(2)−Se(4)	90.85(7)	Se(5)−Bi(2)−Se(4)	90.76(5)
Se(5)−Bi(2)−Se(5)	97.1(1)	Se(5)−Bi(2)−Se(5)	97.20(8)
Se(5)−Bi(2)−Se(4)	171.96(8)	Se(5)−Bi(2)−Se(4)	172.00(5)
Se(7)−Bi(3)−Se(7)	80.18(9)	Se(7)−Bi(3)−Se(7)	80.42(6)
Se(8)−Bi(3)−Se(9)	90.73(9)	Se(8)−Bi(3)−Se(9)	90.64(7)
Se(8)−Bi(3)−Se(8)	97.1(1)	Se(8)−Bi(3)−Se(8)	97.04(9)
Se(8)−Bi(3)−Se(7)	171.41(8)	Se(8)−Bi(3)−Se(7)	171.57(6)
Se(10)−Bi(4)−Se(10)	80.32(9)	Se(10)−Bi(4)−Se(10)	80.12(6)
Se(11)−Bi(4)−Se(10)	90.50(7)	Se(11)−Bi(4)−Se(10)	90.63(5)
Se(11)−Bi(4)−Se(11)	97.0(1)	Se(11)−Bi(4)−Se(11)	96.97(8)
Se(12)−Bi(4)−Se(9)	176.1(1)	Se(12)−Bi(4)−Se(9)	174.28(8)
Se(10)−Bi(5)−Se(4)	86.88(9)	Se(10)−Bi(5)−Se(4)	86.62(7)
Se(2)−Bi(5)−Se(10)	90.51(9)	Se(2)−Bi(5)−Se(10)	91.73(7)
Se(2)−Bi(5)−Se(3)	95.43(9)	Se(2)−Bi(5)−Se(3)	95.34(7)
Se(2)−Bi(5)−Se(4)	176.4(1)	Se(2)−Bi(5)−Se(4)	177.69(8)
Se(7)−Bi(6)−Se(7)	85.38(9)	Se(7)−Bi(6)−Se(7)	85.40(7)
Se(6)−Bi(6)−Se(6)	90.8(1)	Se(6)−Bi(6)−Se(6)	91.24(8)
Se(6)−Bi(6)−Se(7)	93.57(9)	Se(6)−Bi(6)−Se(7)	93.46(7)
Se(6)−Bi(6)−Se(7)	177.94(9)	Se(6)−Bi(6)−Se(7)	177.56(6)
Se(4)−Bi(7)−Se(7)	84.07(8)	Se(4)−Bi(7)−Se(7)	84.66(7)
Se(9)−Bi(7)−Se(4)	89.76(7)	Se(9)−Bi(7)−Se(4)	89.83(5)
Se(10)−Bi(7)−Se(9)	94.03(9)	Se(10)−Bi(7)−Se(9)	93.46(7)
Se(10)−Bi(7)−Se(7)	175.7(1)	Se(10)−Bi(7)−Se(7)	176.85(8)
Se(13)−Bi(8)−Se(12)	79.19(9)	Se(13)−Bi(8)−Se(12)	79.95(7)
Se(13)−Bi(8)−Se(13)	85.19(9)	Se(13)−Bi(8)−Se(13)	84.93(7)
Se(13)−Bi(8)−Se(13)	90.47(9)	Se(13)−Bi(8)−Se(13)	90.54(8)
Se(13)−Bi(8)−Se(12)	164.4(1)	Se(13)−Bi(8)−Se(12)	164.88(9)

where the alkali metals reside are of different size. Also, due to the larger size of the Rb^+ and Cs^+ ions there is no mixed occupancy between the alkali metals and the Bi atoms in $A_2Bi_8Se_{13}$ (A = Rb, Cs), whereas in β-$K_2Bi_8Se_{13}$ several sites exhibit mixed K^+/Bi^{3+} occupancy. It is therefore apparent that the ability of K and Bi atoms to occupy the same crystallographic sites is probably the origin of stability of the β-$K_2Bi_8Se_{13}$ structure. It may also be a crucial factor in determining the electrical properties of the K analogue, which has been shown to be a promising thermoelectric material.[4] $A_2Bi_8Se_{13}$ (A = Rb, Cs) contains an Sb_2Se_3-type fragment that is not found in β-$K_2Bi_8Se_{13}$ but exists in α-$K_2Bi_8Se_{13}$. Although the arrangement of the building blocks in $A_2Bi_8Se_{13}$ (A = Rb, Cs) and α-$K_2Bi_8Se_{13}$ is similar, α-$K_2Bi_8Se_{13}$ does not have NaCl-type blocks but consists only of Sb_2Se_3-, CdI_2-, and Bi_2Te_3-type fragments.

$CsBi_{3.67}Se_6$. $CsBi_{3.67}Se_6$ adopts the structure of α-$CsPbBi_3Se_6$,[10] which consists of building blocks of NaCl-type as those found in $A_2Bi_8Se_{13}$ but is more narrow (2 × 2); see Figure 3. These blocks have the shape of infinite rods that run parallel to the *b*-axis and share edges as each rod is rotated with respect to its neighbors, by ~13°. This rotation results in a corrugated arrangement of the NaCl-type rods in the *ab*-plane. The Cs^+ ions reside in tricapped trigonal prismatic sites with Cs−Se distances 3.672(4)−3.997(4) Å (Table 8).

All bismuth atoms are in octahedral coordination, again with varying degrees of distortion, as observed in $A_2Bi_8Se_{13}$. The Bi(1) atom that is situated in the center of the NaCl-type block is the least distorted with distances of 2.908(2)−3.003(2) Å and angles between 86.74(6) and 92.23(7)°. The Bi(2) octahedron is distorted toward a square pyramid with four bonds between 2.964(2) and 3.001(2) Å, one short at 2.728(3) Å, and

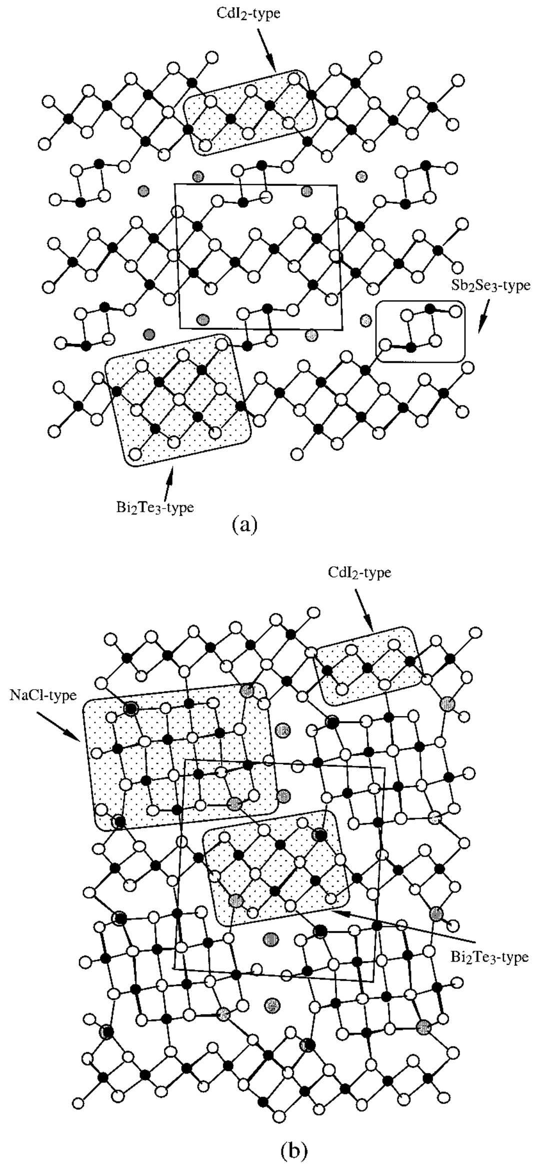

Figure 2. Projection of the structures of (a) α-$K_2Bi_8Se_{13}$ down the *c*-axis and (b) β-$K_2Bi_8Se_{13}$ down the *b*-axis.

one long at 3.141(3) Å. The Bi(3) and Bi(4) octahedra exhibit different kinds of distortion. The Bi(3) octahedron has two short bonds at 2.778(2) Å, two bonds between 2.985(3) and 3.045(3) Å, and two long bonds at 3.199(2) Å resulting in a distortion toward a seesaw environment. The Bi(4) octahedron is the most distorted approaching a trigonal pyramid and is responsible for the zigzag arrangement of the NaCl-type blocks in the structure. It has three short bonds between 2.767(2) and 2.850(3) Å, three long ones between 3.166(2) and 3.172(4) Å, and Se−Bi−Se angles varying between 81.80(8) and 103.98(8)°. To maintain charge neutrality, the Bi(4) sites, which connect the NaCl-type rods, are only 2/3 occupied. By comparison, in α-$CsPbBi_3Se_6$, these positions are fully occupied and the charge balance is maintained by Pb^{2+}.[40]

(40) This suggests that, in α-$CsPbBi_3Se_6$, the Bi(4) site is more likely to be a Pb atom with the rest of the sites being Bi atoms. However, a disorder of Pb/Bi atoms over all metal sites in the structure cannot be ruled out since Pb and Bi due to their close chemical resemblance and similar X-ray scattering properties cannot be crystallographically distinguished.

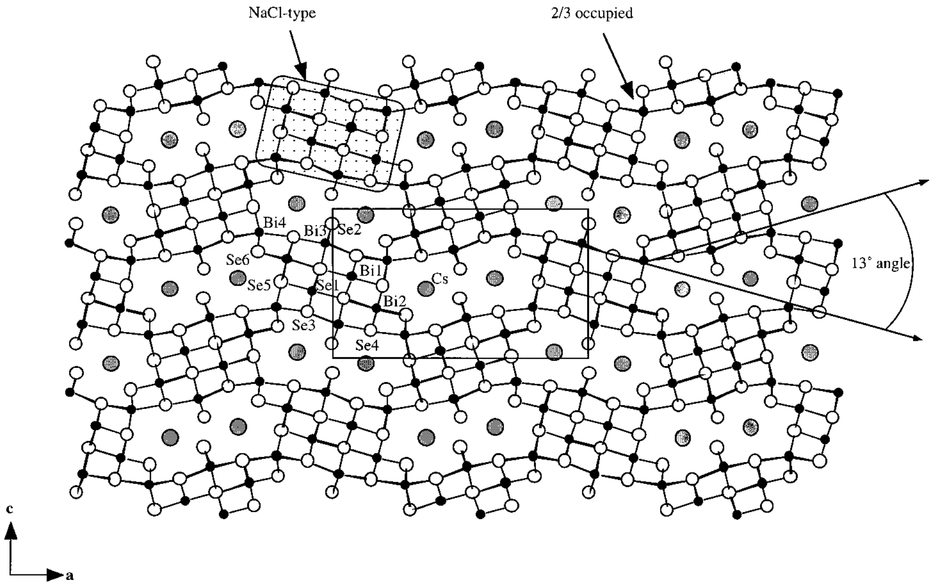

Figure 3. Projection of the structure of $CsBi_{3.67}Se_6$ down the *b*-axis. The shaded areas indicate the NaCl-type building blocks.

Table 8. Bond Distances (Å) and Selected Angles (deg) for $CsBi_{3.67}Se_6$

Bi(1)−Se(3)	2.908(1) × 2	Se(1)−Bi(1)−Se(1)	86.74(6)
Bi(1)−Se(5)	2.939(3)	Se(3)−Bi(1)−Se(5)	92.23(7)
Bi(1)−Se(1)	2.965(3)	Se(5)−Bi(1)−Se(1)	178.13(8)
Bi(1)−Se(1)	3.003(2) × 2		
Bi(2)−Se(6)	2.728(3)	Se(5)−Bi(2)−Se(1)	88.10(7)
Bi(2)−Se(4)	2.964(2) × 2	Se(6)−Bi(2)−Se(4)	92.06(8)
Bi(2)−Se(5)	3.001(2) × 2	Se(4)−Bi(2)−Se(5)	178.12(9)
Bi(2)−Se(1)	3.141(3)		
Bi(3)−Se(2)	2.778(2) × 2	Se(1)−Bi(3)−Se(1)	81.77(6)
Bi(3)−Se(4)	2.985(3)	Se(2)−Bi(3)−Se(2)	97.82(9)
Bi(3)−Se(3)	3.045(3)	Se(2)−Bi(3)−Se(1)	170.71(7)
Bi(3)−Se(1)	3.199(2) × 2		
Bi(4)−Se(6)	2.767(2) × 2	Se(6)−Bi(4)−Se(3)	81.80(8)
Bi(4)−Se(3)	2.850(3)	Se(5)−Bi(4)−Se(4)	103.98(8)
Bi(4)−Se(5)	3.166(2) × 2	Se(6)−Bi(4)−Se(5)	167.4(1)
Bi(4)−Se(4)	3.172(4)		
Cs−Se(2)	3.666(4)		
Cs−Se(6)	3.682(3) × 2		
Cs−Se(4)	3.732(3) × 2		
Cs−Se(2)	3.841(3) × 2		
Cs−Se(3)	3.843(3)		
Cs−Se(5)	3.993(4)		

$BaBi_2Se_4$. This compound adopts the hexagonal β-$BaBi_2S_4$[21] structure type and consists of CdI_2-type and NaCl-type infinite rods, as shown in Figure 4. α-$BaBi_2S_4$[21] has a similar structure, but the NaCl part is shorter in length. Similar NaCl-type blocks with the same thickness but different lengths are also found in $SrBiSe_3$[22] and $BaBiQ_3$[6,24] (Q = Se, Te). Several other compounds such as $SrBi_2S_4$[21] and $EuBi_2S_4$[41] adopt the same structure type whose main characteristic is the existence of tunnels that are partially occupied by the divalent atoms. These tunnels are located at the cell edges parallel to the *c*-axis and form by connecting six narrow (2 Bi atom wide) CdI_2-type one-dimensional infinite rods. The tunnels have 6_3 screw axes running through them. This structure type presents some intricate features, which have not been discussed earlier in the literature.

All Bi atoms have distorted octahedral coordination, similar to what is found in the compounds described above. Bi(1) and Bi(2) in the interior of the NaCl-type fragment have a similar distortion, i.e., toward a square pyramid. Bi(1) has one short Bi−Se bond at 2.703(1) Å, four bonds between 2.917(1) and 3.054(1) Å, and one long Bi−Se distance at 3.516(2) Å. Similarly, Bi(2) has a short bond at 2.664(1) Å, four bonds between 2.8278(9) and 3.179(1) Å, and a long Bi−Se distance at 3.505(1) Å. Bi(3) and Bi(4) are less distorted with Bi−Se distances of 2.791(1)−3.057(1) Å and 2.858(2)−3.026(1) Å, respectively.

(41) Lemoine, P.; Carre, D.; Guittard, M. *Acta Crystallogr.* **1986**, *C42*, 259−261.

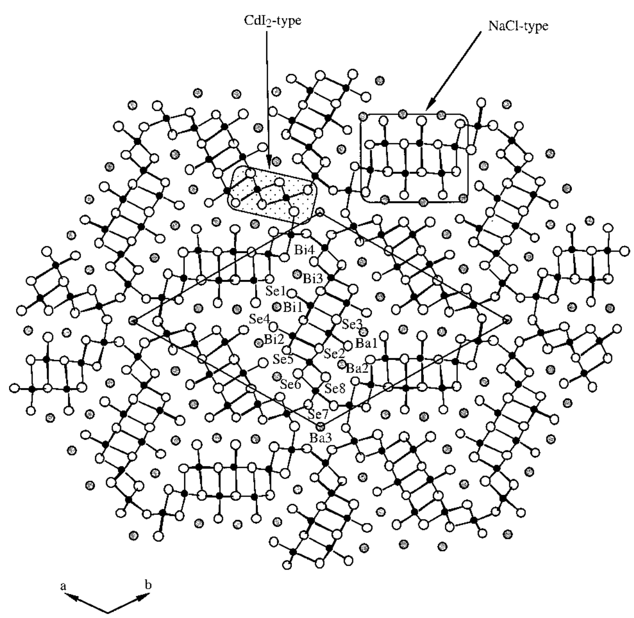

Figure 4. Projection of the structure of $BaBi_2Se_4$ down the *c*-axis. The shaded areas indicate the NaCl-and CdI_2-type building blocks.

The Ba atoms that reside between the NaCl-type blocks have a bicapped trigonal prismatic coordination with Ba−Se distances between 3.268(1) and 3.607(2) Å for Ba(1) and 3.246(1) and 3.480(2) Å for Ba(2). The Ba(3) atom situated in the tunnels interacts with Se(7) (and its symmetry equivalents) and has three distances at 3.083(2) Å and six distances at 3.766(2) Å, adopting essentially a tricapped trigonal prismatic coordination

Table 9. Bond Distances (Å) and Selected Angles (deg) for $BaBi_2Se_4$

Bi(1)−Se(1)	2.703(1)	Se(2)−Bi(1)−Se(3)	85.68(3)
Bi(1)−Se(3)	2.917(1) × 2	Se(3)−Bi(1)−Se(3)	95.70(4)
Bi(1)−Se(2)	3.054(1) × 2	Se(3)−Bi(1)−Se(2)	175.07(4)
Bi(1)−Se(3)	3.516(2)		
Bi(2)−Se(4)	2.664(1)	Se(3)−Bi(2)−Se(2)	84.02(3)
Bi(2)−Se(5)	2.8278(9) × 2	Se(4)−Bi(2)−Se(3)	95.05(3)
Bi(2)−Se(3)	3.179(1) × 2	Se(4)−Bi(2)−Se(2)	178.72(4)
Bi(2)−Se(2)	3.505(1)		
Bi(3)−Se(8)	2.791(1)	Se(6)−Bi(3)−Se(5)	80.46(3)
Bi(3)−Se(6)	2.9246(9) × 2	Se(6)−Bi(3)−Se(6)	95.35(4)
Bi(3)−Se(2)	2.997(1) × 2	Se(6)−Bi(3)−Se(2)	175.89(4)
Bi(3)−Se(5)	3.057(1)		
Bi(4)−Se(7)	2.858(2)	Se(7)−Bi(4)−Se(7)	82.38(8)
Bi(4)−Se(7)	2.861(1) × 2	Se(7)−Bi(4)−Se(7)	98.20(6)
Bi(4)−Se(6)	2.963(1)	Se(7)−Bi(4)−Se(6)	173.54(6)
Bi(4)−Se(8)	3.026(10) × 2		
Ba(1)−Se(1)	3.268(1) × 2		
Ba(1)−Se(4)	3.285(1) × 2		
Ba(1)−Se(4)	3.354(1) × 2		
Ba(1)−Se(5)	3.435(2)		
Ba(1)−Se(3)	3.607(2)		
Ba(2)−Se(1)	3.246(1) × 2		
Ba(2)−Se(8)	3.303(1) × 2		
Ba(2)−Se(6)	3.363(1) × 2		
Ba(2)−Se(2)	3.441(2)		
Ba(2)−Se(5)	3.480(2)		
Ba(3)−Se(7)	3.083(2) × 3		
Ba(3)−Se(7)	3.766(2) × 6		
Ba(3)−Ba(3)	2.1623(2) × 2		

(Table 9). Both Ba(3) and Se(7) have one large anisotropic displacement parameter, U_{22} for Ba(3) and U_{11} for Se(7). This is because the Ba(3) is partially occupied and generates a symmetry equivalent at 2.1623(2) Å away. The full theoretical occupancy for the Ba(3) site is 0.16667, but since this creates symmetry equivalent atoms at a close distance, the maximum allowed occupancy is 0.08333 (50%). The observed occupancy was 0.07266, which corresponds to 44% of the full occupancy of this site. The final formula of the compound is $Ba_{1.07}Bi_2Se_4$, resulting in an excess of 0.07 Ba^{2+} or 0.14 positive charge/formula. This excess of Ba (0.07) corresponds to the Ba atoms found inside the tunnels. If we assume that the atomic sites elsewhere in the structure are fully occupied, then the charge is balanced (i.e. $BaBi_2Se_4$) and the Ba atoms in the tunnels are not needed. The same degree of excess metal cations was also found in $EuBi_2S_4$ and β-$BaBi_2S_4$, which actually have crystallographically refined formulas $Eu_{1.1}Bi_2S_4$ and $Ba_{1.07}Bi_2S_4$, respectively. Attempts to refine the occupancy of the other metal positions in the $BaBi_2Se_4$ structure did not reveal any specific atomic sites to have vacancies. However if the vacancies needed to neutralize the 0.07 Ba^{2+} charge were distributed over all metal sites, their effect on the diffraction properties would be almost negligible making it extremely difficult to detect them by X-ray crystallography. If we accept that $Ba_{1.07}Bi_2Se_4$ is the correct formula, then the $[Bi_2Se_4]$ framework is partially reduced and this should lead to a metallic material. This not the case, however, as the material exhibits an energy band gap and its electrical conductivity is only moderate in the range of semiconductors. On the basis of these observations, we believe the existence of these partially occupied channels is important for the stabilization of the structure.

Energy Gaps. All compounds described here are semiconductors as indicated by the presence of energy gaps detected directly by infrared spectroscopy. Both $Rb_2Bi_8Se_{13}$ and $Cs_2Bi_8Se_{13}$ have a clear band gap of ~0.45 eV whereas the gap is greater for $CsBi_{3.67}Se_6$, at ~0.53 eV, and smaller for $BaBi_2Se_4$, at ~0.32 eV; see Figure 5. The origin of these electronic transitions is thought to be similar to that in Bi_2Se_3, which involves charge transfer from Se p-levels in the valence band to low-lying empty Bi^{3+} p-orbitals in the conduction band. $Rb_2Bi_8Se_{13}$ and $Cs_2Bi_8Se_{13}$ have lower band gaps compared to α- and β-$K_2Bi_8Se_{13}$, which at room temperature have gaps of ~0.76 and ~0.59 eV, respectively.

$CsBi_{3.67}Se_6$ has a band gap very similar to that of the isostructural α-$CsPbBi_3Se_6$, which is ~0.55 eV. Interestingly, the band gap of $BaBi_2Se_4$ is very close to that of Bi_2Se_3 (0.26 eV). The size of the band gap in $CsBi_{3.67}Se_6$ and $Cs_2Bi_8Se_{13}$ seems to correlate with the $Cs_2Se{:}Bi_2Se_3$ ratio in their formula so that as the ratio decreases the band gap also decreases. This relationship has been discussed more extensively in the A_2Q/CdQ systems.[42]

Charge Transport Properties. Temperature-dependent electrical conductivity and thermoelectric power measurements were carried out on single crystals and polycrystalline oriented ingots (grown by the Bridgman technique)[43] of $Rb_2Bi_8Se_{13}$ and $Cs_2Bi_8Se_{13}$. The measurements were taken along the needle axis. The conductivity of single crystals of $Rb_2Bi_8Se_{13}$ is generally low with room-temperature values of ~10 S/cm; see Figure 6. However, the conductivity tended to vary somewhat from specimen to specimen reflecting differences in the doping state, which may arise from inadvertent inhomogeneities in the reaction mixture from which the crystals form. That these differences in conductivity are real and do not represent fluctuations in the experimental procedure are evident from the corresponding changes in thermopower. The conductivity of an oriented ingot of $Rb_2Bi_8Se_{13}$ was slightly greater with a room-temperature value of ~30 S/cm; see Figure 7. For the samples with low conductivity, the thermopower showed both very high positive and sometimes high negative values, even for samples from the same batch. The room-temperature values were ~+650 μV/K for the p-type sample and −200 μV/K for the n-type sample; see Figures 6 and 7. When higher values of conductivity ~80 S/cm were observed in different batches of $Rb_2Bi_8Se_{13}$, the thermopower was lower, ~ −65 μV/K; see Figure 8. Nevertheless, all the conductivity plots have the same features having a slope change around 100 K and reaching a maximum at low temperatures below 50 K. Although the values of electrical conductivity and thermopower are characteristic of semiconductors, the temperature dependence of electrical conductivity and thermopower of $Rb_2Bi_8Se_{13}$ show a metal-like behavior, similar to what is observed in narrow band gap semiconductors.

The electrical conductivity of single crystals of $Cs_2Bi_8Se_{13}$ was found to be even lower than the Rb analogue with room-temperature values of ~0.5 S/cm; see Figure 9. As with $Rb_2Bi_8Se_{13}$, samples with both high positive and high negative thermopower were

(42) Axtell, E. A.; Liao, J.-H.; Pikramenou, Z.; Park, Y.; Kanatzidis. M. G. *J. Am. Chem. Soc.* **1993**, *115*, 12191−12192. (b) Axtell, E. A.; Liao, J.-H.; Pikramenou, Z.; Park, Y.; Kanatzidis. M. G. *Chem. Eur. J.* **1996**, *2*, 656−666.
(43) Kyratsi, T.; Chung, D.-Y.; Choi, K.-S.; Dick, J. S.; Chen, W.; Uher, C.; Kanatzidis M. G. *Mater. Res. Soc. Symp Proc.* **2000**, in press.

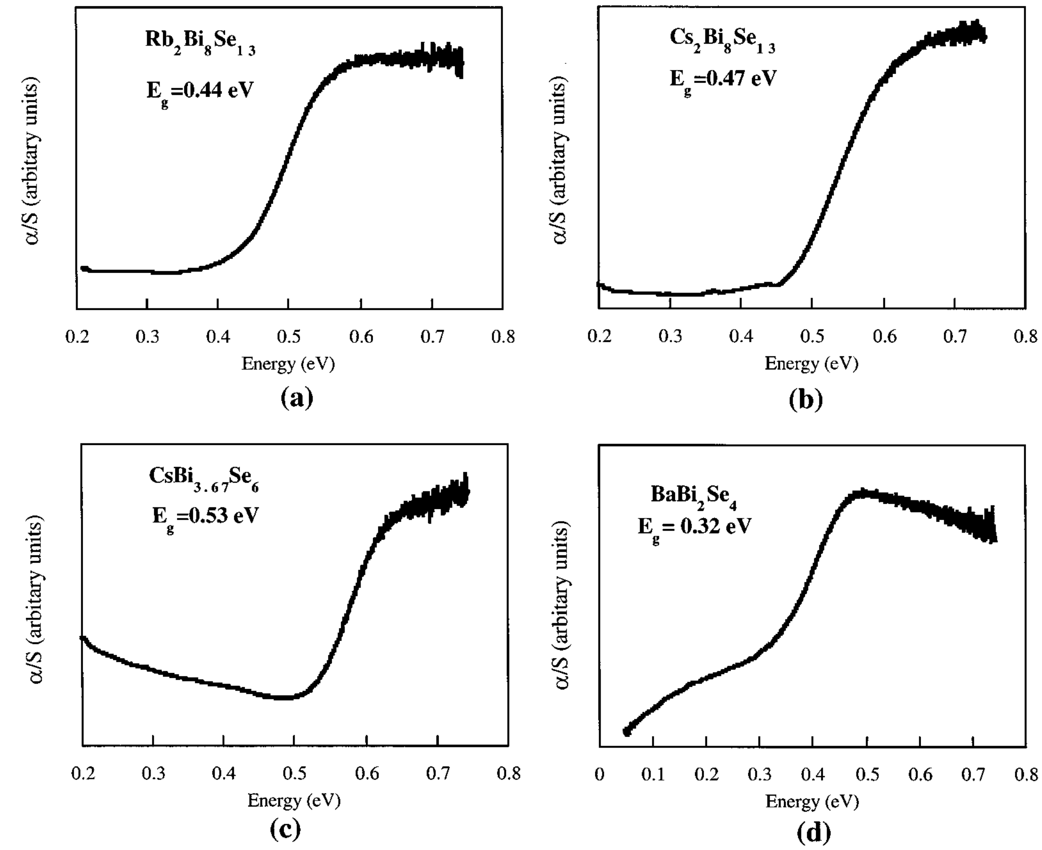

Figure 5. Infrared absorption spectra showing band gap transitions for (a) $Rb_2Bi_8Se_{13}$, (b) $Cs_2Bi_8Se_{13}$, (c) $CsBi_{3.67}Se_6$, and (d) $BaBi_2Se_4$.

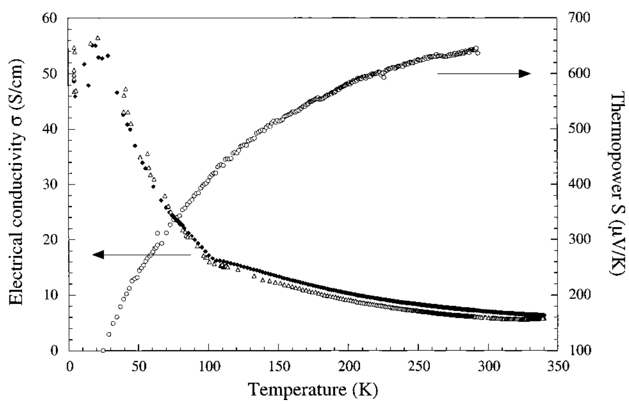

Figure 6. Variable-temperature electrical conductivity and thermopower for single crystals of $Rb_2Bi_8Se_{13}$.

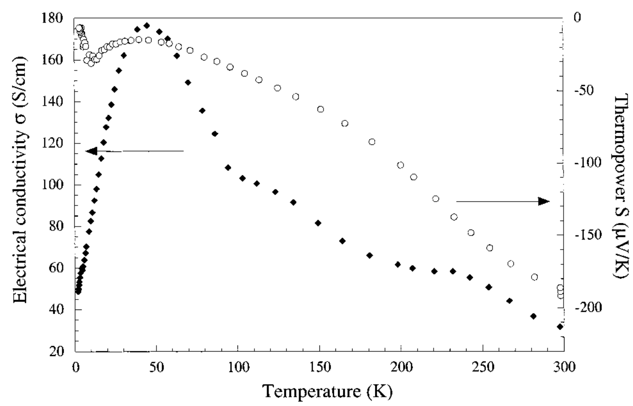

Figure 7. Variable-temperature electrical conductivity and thermopower for oriented polycrystalline samples of $Rb_2Bi_8Se_{13}$.

observed. The room-temperature values were $\sim$+200 μV/K for the p-type sample and $\sim$−300 μV/K for the n-type sample; see Figure 10. The temperature dependences of the electrical conductivity and thermopower are consistent with semiconducting behavior.

The values of electrical conductivity and thermopower for $A_2Bi_8Se_{13}$ (A = Rb, Cs) are similar to those of α-$K_2Bi_8Se_{13}$.[1] Compared to β-$K_2Bi_8Se_{13}$ the $A_2Bi_8Se_{13}$ (A = Rb, Cs) compounds exhibit equal to or greater thermopower but their conductivities are considerably lower. At room temperature the thermopower of β-$K_2Bi_8Se_{13}$[44] is $\sim$−220 μV/K and its electrical conductivity is 250 S/cm. Consequently, the power factor of β-$K_2Bi_8Se_{13}$ (undoped) at 300 K is 12 μW/(cm^2·K) and increasing at higher temperatures, whereas $Rb_2Bi_8Se_{13}$ exhibits a maximum at 150−200 K of only 3.3 μW/(cm^2·K), Figure 11. In summary, β-$K_2Bi_8Se_{13}$ outperforms $Rb_2Bi_8Se_{13}$ in thermoelectric performance mainly because of its higher electrical conductivity. Initial attempts to dope $Rb_2Bi_8Se_{13}$ with Sn and Sb did not drastically change the electrical behavior of the material and were not pursued. If we can improve the electrical conductivity of $Rb_2Bi_8Se_{13}$ through appropriate doping without significant loss in the thermopower, this could be a promising thermoelectric material. An advantage of $A_2Bi_8Se_{13}$ (A = Rb, Cs) over β-$K_2Bi_8Se_{13}$ is that these materials exhibit both an n- and p-type behavior, something that is important in electronics applications.

(44) Brazis, P. W.; Rocci-Lane, M. A.; Ireland, J. R.; Chung, D.-Y.; Kanatzidis, M. G.; Kannewurf, C. R. *Proc. Int. Conf. Thermoelectr.* **1999**, 619−622.

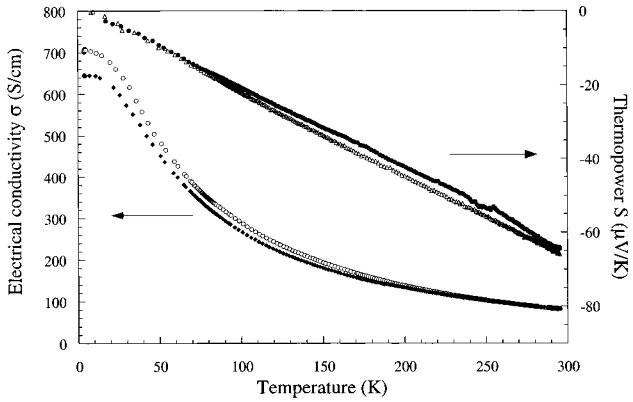

Figure 8. Variable-temperature thermopower for polycrystalline samples of $Rb_2Bi_8Se_{13}$.

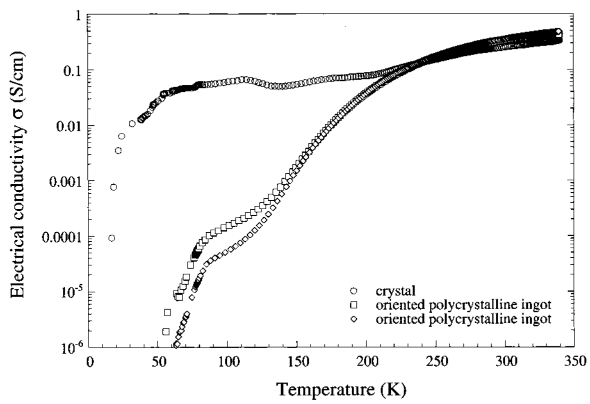

Figure 9. Variable-temperature electrical conductivity for single crystals and oriented polycrystalline samples of $Cs_2Bi_8Se_{13}$.

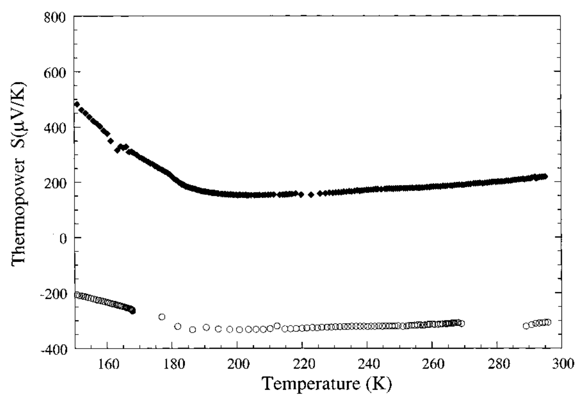

Figure 10. Variable-temperature thermopower for oriented polycrystalline samples of $Cs_2Bi_8Se_{13}$ showing both the n-type and p-type behavior.

Crystals of $CsBi_{3.67}Se_6$ also exhibited a very low room-temperature electrical conductivity similar to those of $A_2Bi_8Se_{13}$ at ~1 S/cm; see Figure 12. The temperature dependence of the conductivity shows signs of thermally activated transport typical of nondegenerate semiconductor. The room-temperature thermopower was ~−160 μV/K; see Figure 13. Some attempts were made to dope $CsBi_{3.67}Se_6$ in order to increase its electrical conductivity. Samples with 0.005 mol % $SbBr_3$ added resulted in an increase of the conductivity to ~20 S/cm at room temperature; see Figure 12. These measurements were done on single crystals of the material prepared by the quenching technique described above. By comparison the isostructural compound α-$CsPbBi_3Se_6$[10] also has a

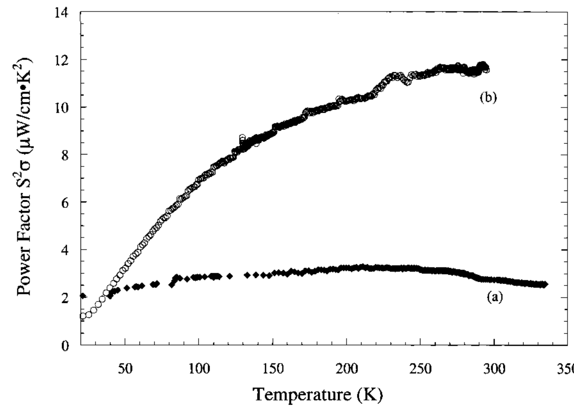

Figure 11. Variable-temperature power factor (σS^2) for (a) $Rb_2Bi_8Se_{13}$ and (b) β-$K_2Bi_8Se_{13}$.

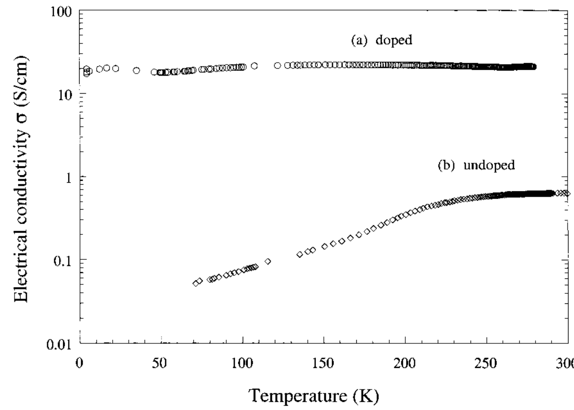

Figure 12. Variable-temperature electrical conductivity for (a) doped with $SbBr_3$ and (b) undoped single crystals of $CsBi_{3.67}Se_6$ prepared by the quenching technique.

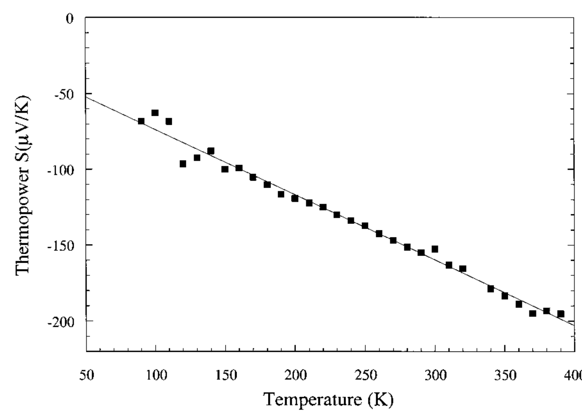

Figure 13. Variable-temperature thermopower for polycrystalline samples of $CsBi_{3.67}Se_6$ prepared by the quenching technique.

low room-temperature conductivity of 0.6 S/cm and a room-temperature thermopower of −730 μV/K. While the conductivity of quenched $CsBi_{3.67}Se_6$ samples is very similar to that of α-$CsPbBi_3Se_6$, their thermopower values are considerably smaller.

For $BaBi_2Se_4$ temperature-dependent electrical conductivity and thermoelectric power measurements were carried out on polycrystalline oriented ingots grown by the Bridgman technique.[43] Again, the measurements were done along the needle (*c*-) axis. The conductivity was higher than those of the previous compounds with a room-temperature value of ~130 S/cm, Figure 14. The thermopower is lower with a room-temperature value

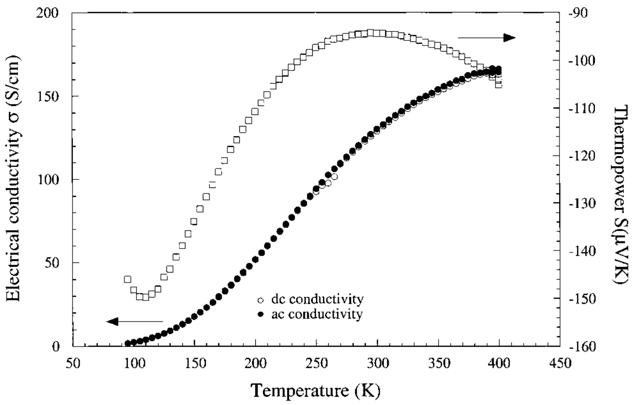

Figure 14. Variable-temperature electrical conductivity and thermopower for an oriented polycrystalline ingot of $BaBi_2Se_4$.

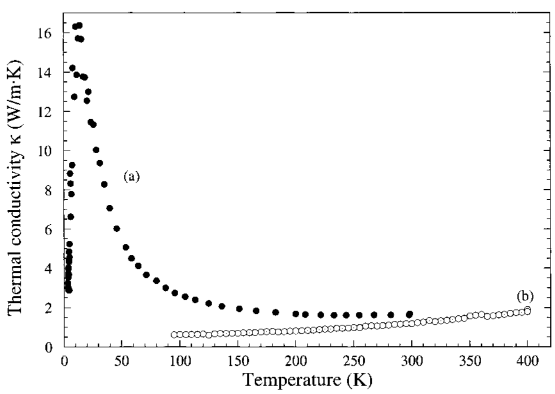

Figure 15. Variable-temperature thermal conductivity for an oriented ingot of (a) $Rb_2Bi_8Se_{13}$ and (b) $BaBi_2Se_4$.

of −95 μV/K, Figure 14. An interesting feature of the thermopower is that it increases as the temperature decreases, reaching a maximum of −150 μV/K at 100 K. The temperature dependence of the electrical conductivity and thermopower indicates that $BaBi_2Se_4$ is an n-type narrow band gap semiconductor.

Thermal Conductivity. The thermal conductivity of $Rb_2Bi_8Se_{13}$ was measured along the growth direction (*b*-axis) on a specimen cut from an oriented ingot. The data are displayed in Figure 15 as a function of temperature from 5 to 300 K. At room temperature the thermal conductivity of $Rb_2Bi_8Se_{13}$ is low with a value of 1.6 W/(m·K). Good crystalline character of the material is revealed by a pronounced peak at low temperature. It arises as a consequence of interplay between the boundary scattering and phonon−phonon Umklapp process.[45] The value of thermal conductivity is very close to that of optimized Bi_2Te_3 alloy (1.5 W/(m·K))[46] and reaffirms the fact that the ternary and quaternary bismuth chalcogenides[3,12,25] can possess very low thermal conductivities. Its thermal conductivity is only slightly higher of that of β-$K_2Bi_8Se_{13}$ which has a value of 1.3−1.4 W/(m·K) at room temperature. The thermal conductivity is dominated by its lattice contribution with the electronic term representing not more than 1% of the total value.

$BaBi_2Se_4$ exhibits a very low thermal conductivity with a room-temperature value of ∼1.2 W/(m·K), Figure 15. Here again the thermal conductivity is essentially due to the lattice contribution.

Concluding Remarks

Four new ternary bismuth chalcogenides have been synthesized: $Rb_2Bi_8Se_{13}$; $Cs_2Bi_8Se_{13}$; $CsBi_{3.67}Se_6$; $BaBi_2Se_4$. All compounds are semiconductors with band gaps between 0.3 and 0.6 eV. $Rb_2Bi_8Se_{13}$ has a very low thermal conductivity of 1.6 W/(m·K) and very high thermopower; however, its electrical conductivity is very low. Clearly its electrical conductivity will have to be improved without a significant loss in thermopower. This however is greatly challenging but could be attempted through doping experiments. Both compounds can exhibit n-type and p-type behavior which, if controllable, is an important property for electronic applications.

$CsBi_{3.67}Se_6$ exhibits n-type semiconducting behavior and has very low electrical conductivity. Doping experiments with $SbBr_3$ increased the electrical conductivity but not sufficiently enough for thermoelectric applications. With its current properties, $CsBi_{3.67}Se_6$ is not a suitable candidate for thermoelectric purposes.

$BaBi_2Se_4$ can be described as an n-type narrow band gap semiconductor and has a very low thermal conductivity of 1.2 W/(m·K), lower than that of optimized Bi_2Te_3. Its thermopower and electrical conductivity values are promising but have to be further improved for thermoelectric applications. The structure type of this compound is attractive because it is very stable and forms with a variety of other metals such Sr and some lanthanides. In addition, the fact that both the S and Se analogues are stable should lead to solid solutions with even lower thermal conductivities.

Acknowledgment. Financial support from the Office of Naval Research (Contract No. N00014-98-1-0443) and ARO-DARPA (M.G.K. and C.U.) is gratefully acknowledged. The work made use of the SEM facilities of the Center for Electron Optics at Michigan State University. The Bruker SMART platform CCD diffractometer at Michigan State University was purchased with funds from the National Science Foundation (Grant CHE-9634638). At NU, this work made use of the Central Facilities supported by the National Science Foundation through the Materials Research Center (Grant DMR-96-32472).

Supporting Information Available: Tables of crystallographic details, atomic coordinates, isotropic and anisotropic displacement parameters for all atoms, structure factors, and interatomic distances and angles for **I**−**IV** (PDF). This material is available free of charge via the Internet at http://pubs.acs.org.

CM000734A

(45) The lattice thermal conductivity follows a T^4 law at very low temperatures and a T^{-1} law at higher temperatures. These different dependencies reflect the contributions of boundary scattering and phonon/phonon Umklapp scattering mechanisms, respectively. Bandari, C., Rowe, M. D. M. *Thermal Conduction in Semiconductors*; Wiley Eastern Ltd.: New Delhi, India, 1988.

(46) *Encyclopedia of Materials Science and Engineering*; *Thermoelectric Semiconductors*; MIT Press and Pergamon Press: Cambridge, MA, Oxford, U.K., 1986; p 4968.